

Theory of Spin Relaxation in Two-Electron Lateral Coupled Si/SiGe Quantum Dots

Martin Raith¹, Peter Stano^{2,3}, and Jaroslav Fabian¹

¹*Institute for Theoretical Physics, University of Regensburg, D-93040 Regensburg, Germany*

²*Institute of Physics, Slovak Academy of Sciences, 845 11 Bratislava, Slovakia*

³*Department of Physics, University of Basel, Klingelberstrasse 82, 4056 Basel, Switzerland*

Highly accurate numerical results of phonon-induced two-electron spin relaxation in silicon double quantum dots are presented. The relaxation, enabled by spin-orbit coupling and the nuclei of ²⁹Si (natural or purified abundance), are investigated for all relevant parameter regimes, the interdot coupling, the magnetic field magnitude and orientation, and the detuning. We calculate all relaxation rates for zero and finite temperatures (100 mK), concluding that all findings for zero temperature qualitatively remain valid also for 100 mK. We confirm the same anisotropic switch of the axis of prolonged spin lifetime with varying detuning as recently predicted in GaAs. However, there is a striking difference compared to the GaAs counterpart. In silicon, the hyperfine-induced relaxation rate is negligible in all cases we studied—even for natural silicon. The spin-orbit coupling, although weak, is the dominant contribution, yielding anisotropic relaxation rates of at least two orders of magnitude lower than in GaAs.

PACS numbers: 72.25.Rb, 03.67.Lx, 71.70.Ej, 73.21.La

I. INTRODUCTION

Since the proposal of Loss and DiVincenzo,¹ electron spins in semiconductor quantum dots have been in the perpetual focus of research on spintronics.^{2,3} In GaAs based qubits, which are the state of the art, the essential gate operations^{4–7} for quantum computation^{8,9} have been demonstrated.^{10–14} But GaAs possesses a serious handicap for coherent spin manipulations—the nuclear spins.^{15,16} Controlling this source of decoherence is of major interest and an active field of research.^{17–22}

An alternative to III-V semiconductors with inherent nuclear spins are systems composed of atoms without nuclear magnetic moment, such as Si and C.^{23–25} Natural silicon consists of three isotopes: ²⁸Si (92.2%), ²⁹Si (4.7%), and ³⁰Si (3.1%).²⁶ Hereof only ²⁹Si has non-zero nuclear spin ($I=1/2$), and purification can further reduce its abundance down to 0.05%.^{27,28} For this reason, silicon-based quantum dots have become the new focus of interest, and recent progress emphasizes their perspectives.^{29–32} Another advantage of silicon^{9,25} over GaAs is a larger g factor, which allows spin manipulations in smaller magnetic fields. On the other hand, device fabrication of silicon dots is more challenging,³³ the spin-orbit interactions are weaker, and the dots must be smaller due to a larger effective mass.

Bulk silicon has six equivalent conduction band minima located on the Δ -lines, at $k_v \approx 0.84k_0$ toward the six X points of the Brillouin zone, where $k_0 = 2\pi/a_0$ with $a_0 = 5.4 \text{ \AA}$ the lattice constant.^{34–36} They are typically referred to as Δ -valleys or X -valleys. In general, their degeneracy is lifted by strain, or by the presence of an interface.^{35,37} In a (001)-grown silicon heterostructure, the four in-plane valleys are split by at least 10 meV from the two lower-lying $\pm z$ valleys, resulting in a twofold conduction band minimum. This remaining degeneracy is further split if the perpendicular confinement is asymmetric, resulting in an energy difference

called the ground state gap.^{38–45} As the valley degeneracy is believed to be the main obstacle for silicon-based quantum computation^{42,46,47}, a large valley splitting is desired. If this is the case, the multi-valley system can be reduced to an effective single valley qubit, a potentially nuclear-spin-free analog to the well-known GaAs counterpart.^{46,47} In fact, many recent experiments performed on Si/SiGe quantum dots have no evidence of valley degeneracy,^{29–31,48–50} indicating that the splitting is large enough to justify a single valley treatment. On the other hand, a recent proposal of valley-defined qubits uses the valley degree of freedom as a tool for gate operations.⁵¹ This requires precise control of the ground-state gap, a challenging task for the future. In this work we assume that the valley splittings are larger than the typical energy scale of interest so that the effective single valley approximation is valid.

The spin relaxation and decoherence has been investigated theoretically and experimentally in silicon-based single and double dots from single to many electron occupancy.^{30,31,46,49,50,52–63} Our work completes these findings by a global, quantitative understanding of two-electron lateral silicon double quantum dots. We investigate the spin-orbit and hyperfine induced relaxation rate as a function of interdot coupling, detuning, and magnitude and orientation of the external magnetic field for zero and finite temperatures, and for natural and isotopically purified silicon. We pay special attention to the spin hot spots⁶⁴, and investigate individual relaxation channels. We assume the double dot orientation with respect to the crystallographic axes that is used most often in experiments. This work is an extension to the findings in Ref. 65 for GaAs, and we highlight the differences between these two materials.

We find that due to the small spin-orbit coupling the spin relaxation rates are typically at least two orders of magnitude lower than in comparable GaAs dots, and that the relaxation rate peaks at spin hot spots are very nar-

row in parameter space. For detuned double dots, the energy spectrum close to the singlet-singlet anticrossing is qualitatively different from the GaAs counterpart, due to the rather small single-dot exchange coupling compared to the anticrossing energy. We also find that the hyperfine-induced relaxation rates of natural silicon are at least two orders of magnitude lower than the spin-orbit induced relaxation rates, even for the unpolarized triplet of detuned double dots contrariwise to GaAs.⁶⁵ The hyperfine-induced rates of purified silicon are, again, about two orders of magnitude lower compared to natural silicon. We conclude that, concerning the relaxation, the nuclear field is negligible. Thus, the anisotropy of the spin-orbit field manifests in all relaxation rates we calculated, yielding the electrically controlled directional switch of the easy passage⁶⁶ (a particular orientation of the magnetic field for which the relaxation as a function of some parameter is significantly lower than for other orientations), previously found in GaAs.⁶⁵ A temperature of 0.1 K does not change our findings in any qualitative way. We give quantitative results for experimentally realistic parameters covering the whole experimentally significant range of the parametric space.

II. MODEL

We consider a $\hat{z} = [001]$ grown top-gated Si/SiGe heterostructure defining a laterally coupled double quantum dot within the silicon layer with a fraction of ^{29}Si isotopes. The double dot is charged with two electrons and not coupled to leads. Assuming the validity of the effective single valley approximation,⁵⁸ the Hamiltonian in the two-dimensional and the envelope function approximation reads

$$H = \sum_{i=1,2} (T_i + V_i + H_{Z,i} + H_{\text{so},i} + H_{\text{nuc},i}) + H_C. \quad (1)$$

The operators of position \mathbf{r} and momentum \mathbf{P} are two-dimensional, where $\hat{x} = [100]$ and $\hat{y} = [010]$. The single-electron terms are labeled by the electron index i . The kinetic energy is $T = \mathbf{P}^2/2m$, with the kinetic momentum $\mathbf{P} = -i\hbar\nabla + e\mathbf{A}$, the effective electron mass m , and the electron charge $-e$. For an external magnetic field, given by $\mathbf{B} = (B_{\parallel} \cos \gamma, B_{\parallel} \sin \gamma, B_z)$, where γ is the angle between the in-plane component of \mathbf{B} and \hat{x} , the vector potential in symmetric gauge reads $\mathbf{A} = B_z(-y, x)/2$. We neglect the orbital effects of the in-plane magnetic field component, which is a good approximation up to roughly 10 T for common heterostructures.⁶⁷ The electrostatic potential,

$$V = \frac{\hbar^2}{2ml_0^4} \min\{(\mathbf{r} - \mathbf{d})^2, (\mathbf{r} + \mathbf{d})^2\} + e\mathbf{E} \cdot \mathbf{r}, \quad (2)$$

consists of the biquadratic confinement^{47,68} and the external electric field. For $\mathbf{E} = 0$, the potential is minimal at $\pm\mathbf{d}$, calling $2d/l_0$ the interdot distance. The single dot scale is given by the confinement length l_0 , and

equivalently by the confinement energy $E_0 = \hbar^2/(ml_0^2)$. The electric field \mathbf{E} is applied along the dot main axis \mathbf{d} , where the angle δ gives the in-plane orientation with respect to \hat{x} . Turning on \mathbf{E} shifts the potential minima relative to each other by the detuning energy $\epsilon = 2eEd$. The geometry is plotted in Fig. 1 of Ref. 69.

The Zeeman term is $H_Z = (g/2)\mu_B\boldsymbol{\sigma}\cdot\mathbf{B}$, with the vector of Pauli matrices $\boldsymbol{\sigma} = (\sigma_x, \sigma_y, \sigma_z)$, the effective Landé factor g , and the Bohr magneton μ_B . The spin-orbit coupling, $H_{\text{so}} = H_{\text{br}} + H_{\text{d}}$, includes the Bychkov-Rashba^{2,70} and the generalized Dresselhaus Hamiltonians,^{2,71-73}

$$H_{\text{br}} = (\hbar/2ml_{\text{br}})(\sigma_x P_y - \sigma_y P_x), \quad (3)$$

$$H_{\text{d}} = (\hbar/2ml_{\text{d}})(-\sigma_x P_x + \sigma_y P_y), \quad (4)$$

parameterized by the spin-orbit lengths l_{br} and l_{d} . In this work we assume interface inversion asymmetry and choose l_{br} and l_{d} of comparable strength, according to Ref. 73. The nuclear spins of ^{29}Si dominantly couple through the Fermi contact interaction^{16,74,75}

$$H_{\text{nuc}} = \beta \sum_n \mathbf{I}_n \cdot \boldsymbol{\sigma} \delta(\mathbf{R} - \mathbf{R}_n), \quad (5)$$

where β is a constant, \mathbf{I}_n is the spin of the n -th nucleus at the position \mathbf{R}_n , and $\mathbf{R} = (\mathbf{r}, z)$ is the three-dimensional electron position operator. Here we need to consider the finite extension of the wavefunction perpendicular to the heterostructure interface. We assume it is fixed to the ground state of a hard-wall confinement of width w . This defines the effective width,

$$h_z = \left[\int dz |\psi(z)|^4 \right]^{-1}, \quad (6)$$

which evaluates to $h_z = 2w/3$. Finally, the Coulomb interaction is $H_C = e^2/4\pi\epsilon|\mathbf{r}_1 - \mathbf{r}_2|$, with the material dielectric constant ϵ .

The energy relaxation is enabled by phonons, whereas spin-orbit interactions allow for a spin-flip. In a (001)-grown quantum well of silicon, the electron-phonon coupling for intravalley scattering is the deformation potential of transverse acoustic (TA) and longitudinal acoustic (LA) phonons, given by^{56,60,76-79}

$$H_{\text{ep}} = i \sum_{\mathbf{Q}, \lambda} \sqrt{\frac{\hbar Q}{2\rho V c_\lambda}} D_{\mathbf{Q}}^\lambda \left[b_{\mathbf{Q}, \lambda}^\dagger e^{i\mathbf{Q}\cdot\mathbf{R}} - b_{\mathbf{Q}, \lambda} e^{-i\mathbf{Q}\cdot\mathbf{R}} \right], \quad (7)$$

where

$$D_{\mathbf{Q}}^\lambda = (\Xi_{\text{d}} \hat{\mathbf{e}}_{\mathbf{Q}}^\lambda \cdot \hat{\mathbf{Q}} + \Xi_{\text{u}} \hat{\mathbf{e}}_{\mathbf{Q}, z}^\lambda \hat{Q}_z). \quad (8)$$

The phonon wave vector is $\mathbf{Q} = (\mathbf{q}, Q_z)$, and $\hat{\mathbf{Q}} = \mathbf{Q}/Q$. The polarizations are given by⁸⁰ $\lambda = \text{TA1}, \text{TA2}, \text{LA}$, the polarization unit vector reads $\hat{\mathbf{e}}$, and the phonon annihilation (creation) operator is denoted by b (b^\dagger). The mass density, the volume of the crystal, and the sound velocities are given by ρ , V , and c_λ , respectively. The efficiency of the electron-phonon coupling is set by the dilatation and shear potential constants, Ξ_{d} and Ξ_{u} respectively.

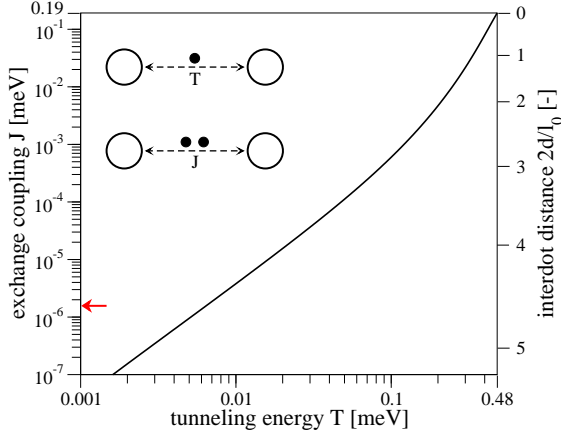


FIG. 1. (Color online) Calculated conversion from single-electron tunneling energy T to two-electron exchange coupling J neglecting nuclear spins. The scale for the interdot distance $2d/l_0$ is also shown. The arrow gives E_{nuc} , Eq. (10), of natural silicon.

We define the relaxation rate (the inverse of the lifetime T_1) as the sum of the individual transition rates to all lower-lying states. Each rate (from $|i\rangle$ to $|j\rangle$) is evaluated using Fermi's Golden Rule at zero temperature,³

$$\Gamma_{ij} = \frac{\pi}{\rho V} \sum_{\mathbf{Q}, \lambda} \frac{Q}{c_\lambda} |D_{\mathbf{Q}}^\lambda|^2 |M_{ij}|^2 \delta(E_{ij} - E_{\mathbf{Q}}^\lambda), \quad (9)$$

where $M_{ij} = \langle i | e^{i\mathbf{Q} \cdot (\mathbf{R}_1 + \mathbf{R}_2)} | j \rangle$ is the matrix element of the states with energy difference E_{ij} , and $E_{\mathbf{Q}}^\lambda$ is the energy of a phonon with wave vector \mathbf{Q} and polarization λ . In this work we focus on the singlet (S) and the three triplets (T_-, T_0, T_+) at the bottom of the energy spectrum.

Our numerical method is discussed in Refs. 81 and 82. The extension to include the hyperfine coupling, Eq. (5), was introduced in Ref. 65. In this work, the two-electron basis for the configuration interaction method consists of 1156 Slater determinants, generated by 34 single-electron orbital states. The discretization grid is typically 135×135 . The relative error for energies is below 10^{-5} . The reliability of our code is confirmed by the evaluation of Eq. (9) in an analytically solvable regime—weakly coupled dots in low magnetic fields. For details on this calculation, see the Appendix.

We use the parameters of a SiGe/Si/SiGe quantum well grown along the $\hat{z} = [001]$ direction with a germanium concentration of 25%. The two-dimensional electron gas is defined in the thin silicon layer with tensile strain.^{34,83} The in-plane effective mass is isotropic, given by the transverse mass of the X valley states,³⁷ and we use $m = 0.198m_e$,⁸⁴ where m_e is the free electron mass. The effective Landé factor is $g = 2$.^{40,85} Other material parameters read $c_l = 9150$ m/s (for LA phonons), $c_t = 5000$ m/s (for TA phonons), $\rho = 2330$ kg/m³, and $\varepsilon = 11.9\varepsilon_0$.⁸⁶ The choice of deformation potential constants is not unique,^{78,79,87} and we use $\Xi_d = 5$ eV and

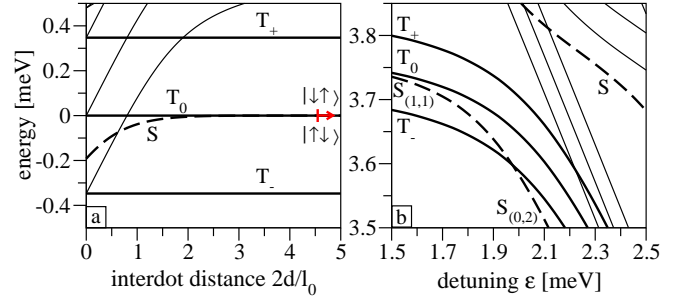


FIG. 2. (Color online) Calculated energies of the lowest states varying (a) the interdot coupling (at $B = 3$ T), and (b) the detuning (at $B = 0.5$ T). Singlet states are given by dashed, triplets by solid lines. In (a), the energy of T_0 is subtracted, and in (b), the quadratic trend in E is subtracted. The arrow in a) marks where $J = E_{\text{nuc}}$ (for natural silicon).

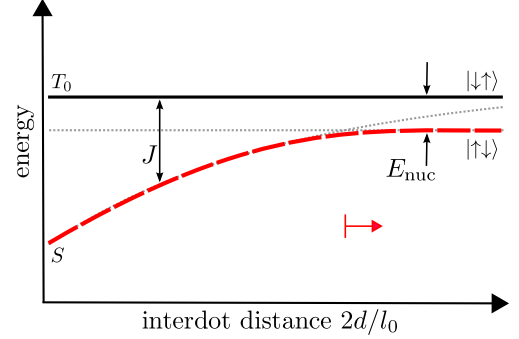


FIG. 3. (Color online) Schematic energy spectrum of an unbiased double dot showing the singlet S (dashed line) and the triplet T_0 (solid line). For large interdot distances, the exchange coupling J is given by the hyperfine splitting E_{nuc} , Eq. (10), and the eigenstates change to $|\downarrow\uparrow\rangle$ and $|\uparrow\downarrow\rangle$.

$\Xi_u = 9$ eV according to Ref. 86. The hyperfine coupling parameter reads $\beta = -0.1 \mu\text{eV nm}^3$, and ^{29}Si has spin $I = 1/2$. For natural silicon, the ^{29}Si abundance is 4.7%, and we use an abundance of 0.05% for purified silicon. For the spin-orbit coupling strength we choose $l_{\text{br}} = 38.5 \mu\text{m}$ and $l_d = 12.8 \mu\text{m}$.^{73,85} The confinement length is $l_0 = 20$ nm ($E_0 = 1.0$ meV), in line with realistic dot sizes.^{49,88} The double dot is oriented as $\mathbf{d} \parallel [110]$. The magnetic field is in-plane unless stated otherwise.

III. RESULTS: UNBIASED DOUBLE DOT

We parameterize in our model the coupling of the double quantum dot by the interdot distance $2d/l_0$. The corresponding experimental observables are the tunneling energy T (single-electron occupancy)^{58,89} and the exchange coupling J (two-electron occupancy).⁸¹ The conversion between these three equivalent parameters is plotted in Fig. 1 for clarity.

The numerically calculated energy spectrum of the unbiased double dot is shown in Fig. 2. In this section, we

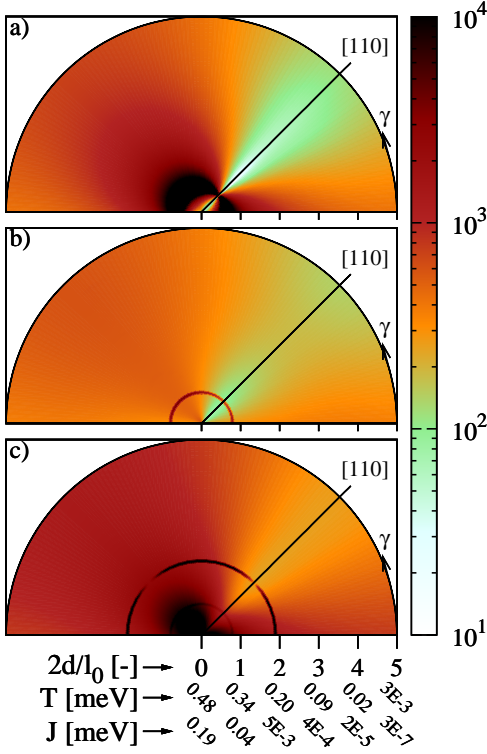


FIG. 4. (Color online) Calculated relaxation rates of (a) the singlet, (b) the triplet T_0 , and (c) the triplet T_+ as a function of the in-plane magnetic field orientation γ (angle) and the interdot distance $2d/l_0$ (radius of the polar plot), for a double dot at $B = 3$ T. The x and y axes correspond to crystallographic axes $[100]$ and $[010]$, respectively. The dot orientation $\mathbf{d} \parallel [110]$ is marked by a line. The x axis is converted to the tunneling energy T and the exchange J , in addition to $2d/l_0$. The rate is given in inverse seconds by the color scale. The system obeys C_{2v} symmetry, so point reflection would complete the graphs.

choose a magnetic field of $B = 3$ T. For the single dot ($d = 0$) the exchange coupling, $J = E(T_0) - E(S)$, is $J_{SD} = 0.19$ meV. The Zeeman energy, $E_Z = g\mu_B B$, exceeds J for magnetic fields beyond 1.7 T. Consequently, we find in Fig. 2a that T_- is the ground state for all interdot distances. The singlet therefore has an anticrossing with an excited triplet in the strong coupling regime, here at $J = 75 \mu\text{eV}$ for our choice of parameters. This scenario is hardly met in comparable GaAs double quantum dots, because the required magnitude of the magnetic field is above 10 T.⁶⁵ The silicon spectrum resembles the GaAs spectrum for magnetic fields below 1.7 T.

At large interdot distances, the hyperfine coupling induces a splitting of S and T_0 , given by

$$E_{\text{nuc}} = 2 \sqrt{\left| \sum_{i=1,2} \langle \phi_a T_0 | H_{\text{nuc},i} | \phi_s S \rangle \right|^2}. \quad (10)$$

In this regime, the lowest eigenstates are $|\uparrow\downarrow\rangle = (S + T_0)/\sqrt{2}$ and $|\downarrow\uparrow\rangle = (S - T_0)/\sqrt{2}$ (c.f. Fig. 3). We evaluate Eq. (10) by averaging over random nuclear spin

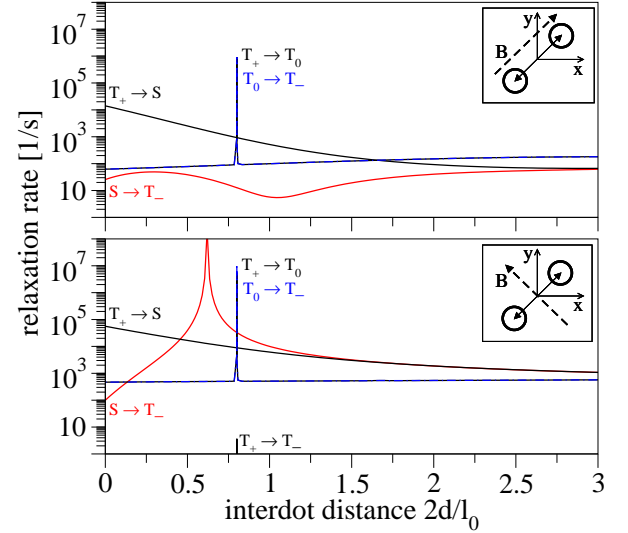


FIG. 5. (Color online) Calculated channel resolved relaxation rates vs. interdot distance for both parallel (top) and perpendicular to \mathbf{d} (bottom) in-plane magnetic field orientation ($B = 3$ T). The relaxation channels of T_+ are black, of T_0 are blue, and of S are red.

ensembles, and obtain $E_{\text{nuc}} \approx 2$ neV for natural, and $E_{\text{nuc}} \approx 0.1$ neV for purified silicon. This implies a crossover to the nuclear dominated regime at $2d/l_0 \gtrsim 4.6$ (red arrows in Figs. 1, 2a, and 3) for natural, and at $2d/l_0 \gtrsim 5.3$ for purified silicon.

We plot the relaxation rates of the states S , T_0 , and T_+ , denoted in Fig. 2, as a function of the interdot distance and in-plane magnetic field orientation in Fig. 4. We also give the relaxation rates of individual channels for the two principal axes, that is for the in-plane magnetic field component parallel and perpendicular to the dot main axis \mathbf{d} , in the upper and lower panel of Fig. 5, respectively. We find that the relaxation rate of the singlet is highly anisotropic due to the effective, spin-orbit induced magnetic field.^{65,66} The rates are minimal if $\mathbf{B} \parallel \mathbf{d}$, reaching the order of tens of milliseconds for any dot coupling strength (Fig. 5). We call this characteristic an easy passage.⁶⁶ In the strong coupling regime, the rate away from the easy passage is enhanced by orders of magnitude. This results from the coupling of the singlet with the excited triplet, which favors the transition into T_- . For $\mathbf{B} \parallel \mathbf{d}$, the rate at the anticrossing is extremely sensitive to variations of γ , such that the easy passage becomes very narrow. A spectral crossing, which is lifted in the presence of spin-orbit coupling, is denoted a spin hot spot.⁶⁴

The relaxation rate of T_0 is given in Fig. 4b. We find the same general anisotropic behavior, which is that the rate is minimal for $\mathbf{B} \parallel \mathbf{d}$. Figure 5 shows that the dominant channel of the relaxation is the transition $T_0 \rightarrow T_-$. Consequently, there is no impact from the singlet-triplet anticrossing. However, the anticrossing of the excited triplet with T_0 itself manifests in a very sharp peak of

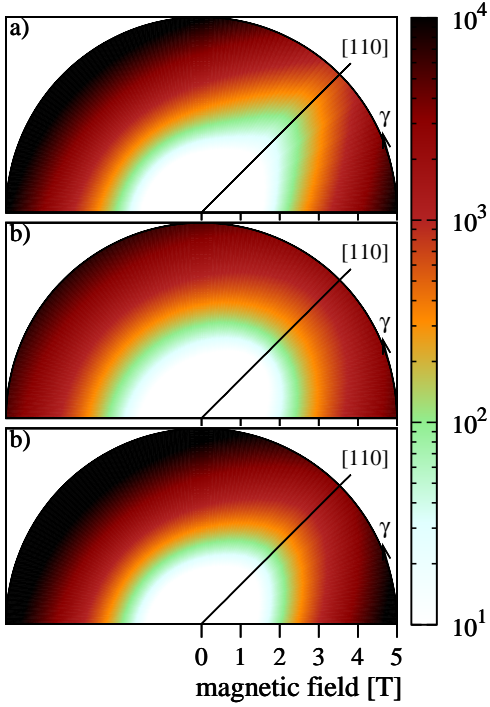


FIG. 6. (Color online) Calculated relaxation rates of (a) the singlet, (b) the triplet T_0 , and (c) the triplet T_+ as a function of the in-plane magnetic field orientation γ (angle) and the magnetic field magnitude (radius of the polar plot), for a double dot with $T = 0.1$ meV. The layout with respect to the crystallographic axes is the same as in Fig. 4. The rate is given in inverse seconds by the color scale.

its rate. This spike is also anisotropic, with a difference of roughly one order of magnitude (not visible in Fig. 4b due to its resolution).

Panel c) of Fig. 4 shows the relaxation rate of T_+ . In addition to the anisotropic background, there are two spikes of enhanced rate generated by the anticrossings of T_+ with the excited triplets. The enhancement close to the single dot regime originates from the dominant $T_+ \rightarrow S$ transition (c.f. Fig. 5). Interestingly, the anticrossing of the singlet hardly influences the overall trend of this relaxation channel.

We plot in Fig. 6 the relaxation rates of a weakly coupled double dot as a function of in-plane magnetic field. Here we find the same qualitative behavior for all three panels. Similarly as in Fig. 4, the relaxation rate is minimal for $\mathbf{B} \parallel \mathbf{d}$, but there are no spin hot-spots here.

IV. RESULTS: BIASED DOUBLE DOT

In this section we consider a weakly coupled double dot with a finite detuning energy ϵ . Figure 7 introduces important characteristic energies in a schematic energy spectrum. The state charge character is given in brackets: (1,1) indicates that there is one electron in each dot,

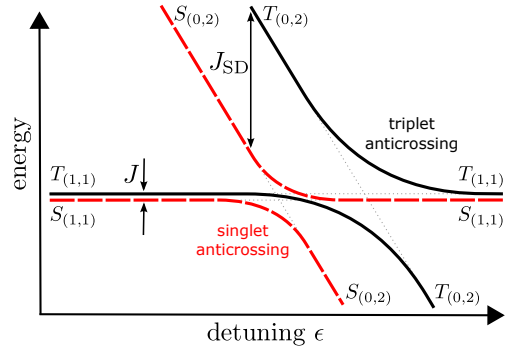


FIG. 7. (Color online) Schematic energy spectrum of a biased double dot without magnetic field. The singlets are given in dashed lines, the triplets in solid lines.

and (0,2) states that both electrons are in the same dot. In the spectra, we subtract the quadratic trend in the electric field E . This way, the (1,1) states are displayed horizontally unless influenced by anticrossings. The important quantities are the single-dot exchange coupling J_{SD} , the double-dot exchange coupling J , and the singlet and triplet anticrossing energy splittings, labeled in Fig. 7 respectively. The single-dot exchange coupling J_{SD} is set by material parameters, i.e. the Coulomb interaction, and system parameters, i.e. the confinement length. For non-interacting electrons, J_{SD} is equal to the confinement energy E_0 , here 1 meV. For interacting particles, the Coulomb repulsion has strong impact on the symmetric ground state, the singlet, as here the electrons tend to group together. The first excited state, the triplet, is antisymmetric with respect to point reflection at the dot origin, and therefore less affected. As a consequence, J_{SD} decreases as the Coulomb interaction strength increases. For our choice of parameters $J_{SD} = 0.2$ meV. In contrast, J_{SD} increases as the confinement length decreases. For instance, a confinement length of $l_0 = 17$ nm results in $J_{SD} \approx 0.3$ meV. This can be understood as follows. On the one hand, a stronger confinement increases the Coulomb strength due to smaller effective particle distances $|\mathbf{r}_1 - \mathbf{r}_2|$ in H_C . This is an effect somewhat linear in l_0^{-1} . Then, one could expect J_{SD} to decrease. However, the confinement energy E_0 scales as l_0^{-2} , by what the exchange coupling increases in a similar way. This scaling dominates, such that the single-dot exchange coupling increases. The double-dot exchange coupling J decreases exponentially with increasing interdot distance d .^{58,89} In the weak coupling regime it holds $J \ll J_{SD}$, and we choose d such that $J = 0.6$ μ eV. The anticrossing gap of a spin-alike pair of states at the $(1,1) \leftrightarrow (0,2)$ transition depends on the interdot distance as well. For increasing d (decreasing J), these gaps decrease, that is the anticrossings vanish as $2d/l_0 \rightarrow \infty$.

The numerically calculated energy spectrum is plotted in Fig. 2b for a magnetic field of $B = 0.5$ T. The spectrum is qualitatively different from the GaAs double dot counterpart (see Fig. 1 in Ref. 65). In a compara-

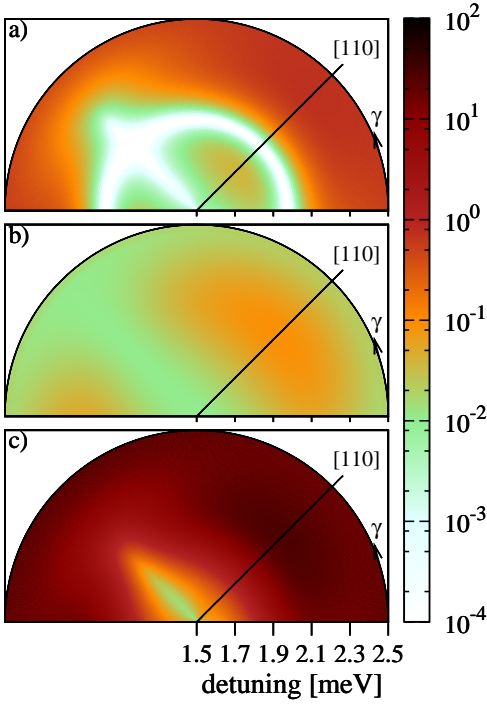


FIG. 8. (Color online) Calculated relaxation rates of (a) the first excited state (S or T_- , see Fig. 2b), (b) T_0 , and (c) T_+ as a function of the in-plane magnetic field orientation γ (angle) and detuning energy (radius of the polar plot), for a double dot with $2d/l_0 = 2.85$ ($T = 0.1$ meV), and $B = 0.5$ T. The layout with respect to the crystallographic axes is the same as in Figs. 4 and 6. The rate is given in inverse seconds by the color scale.

ble GaAs double dot, the singlet and triplet anticrossings gaps are small compared to the single-dot exchange coupling. Consequently, the singlet anticrossing is well separated from the triplet anticrossing, and the excited singlet is close to T_0 in between these anticrossings. In this regime, the relaxation rate is dominated by the coupling between T_0 and the excited singlet, and this coupling is solely due to the nuclear spins.⁶⁵ In silicon (c.f. Fig. 2b) the anticrossings are much more pronounced, and J_{SD} is smaller than in GaAs. Therefore, in the experimentally most relevant detuning energy range up to the triplet-triplet (anti-)crossings, the excited singlet is far away in energy. Thus, there is no significant (hyperfine) coupling between T_0 and the excited singlet, i.e. the relaxation rates are not affected by the excited singlet in any case (see below).

We plot the relaxation rates of the detuned double dot in Fig. 8. Panel a) corresponds to the first excited state, that is S for detuning energies up to 1.97 meV, and T_- beyond. At the singlet-triplet anticrossing, the relaxation rate is very low as the transferred energy becomes very small. The effective, spin-orbit induced, magnetic field,^{65,66} Eq. (12), confirms that the easy passage occurs if the external, in-plane magnetic field is perpendicular to \mathbf{d} . The anisotropy is also visible for the relaxation

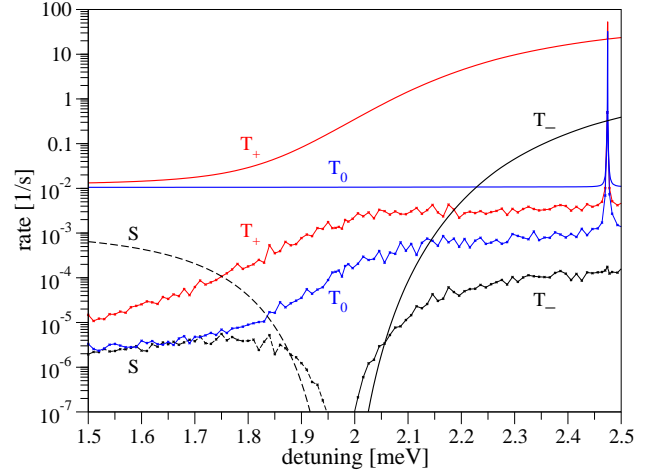


FIG. 9. (Color online) Calculated relaxation rates of a biased double dot in an in-plane magnetic field ($B = 0.5$ T, $\gamma = 3\pi/4$) as a function of detuning. The straight lines give the spin-orbit induced relaxation, the wiggly lines the hyperfine induced relaxation rates (natural silicon).

rates of T_0 and T_+ , panel b) and c) respectively. This directional switch has also been found numerically in GaAs dots.⁶⁵ There is no signature of the singlet-triplet anticrossing in the rate because of the exact compensation of individual relaxation channels.⁶⁵ Also, there is no indication of the crossing of T_+ with the excited triplet T_- . Other anticrossings with excited triplets (at $\epsilon \approx 2.47$ meV) manifest in extremely narrow peaks of the rate, not visible in Fig. 8 at the current resolution.

Let us comment on the role of hyperfine spins. Comparing the interaction strengths with the spin-orbit fields, they are expected to be negligible. Indeed, the Overhauser field characterizing the fluctuating collective nuclear field,¹⁶

$$\mathbf{B}_{\text{nuc}} = \frac{\beta}{g\mu_B} \left\langle \sum_n \mathbf{I}_n |\psi(\mathbf{R}_n)|^2 \right\rangle, \quad (11)$$

of natural silicon is of the order of tens of μT , for purified silicon even one order of magnitude lower. On the other hand, the effective spin-orbit field ($x_d, y_d = (x \pm y)/\sqrt{2}$),⁶⁶

$$\mathbf{B}_{\text{so}} = \mathbf{B} \times \{x_d(l_{br}^{-1} - l_d^{-1})[1\bar{1}0] + y_d(l_{br}^{-1} + l_d^{-1})[110]\}/\sqrt{2}, \quad (12)$$

is about 2 mT at $B = 1$ T. Still, in GaAs we have found that despite a similar discrepancy, there are cases where the nuclear field dominates the spin-orbit field, as the latter is quenched by symmetry imposed selection rules.⁶⁵ Here, however, such anomalous situation does not arise due to the different spectrum, as we discussed above in Sec. IV. The matrix elements of the spin flipping transitions are in Si therefore always dominated by the spin-orbit fields, rather than nuclear spin fields and the same holds for anticrossing gaps. An illustration is given in Fig. 9.

The second possibility we considered, was a dot detuned so far (so small J), that singlet and triplet T_0 become degenerate with respect to E_{nuc} . The Hamiltonian eigenstates change, from entangled states into separable states with spin up or down in the left or right dot respectively (we show this schematically in Fig. 3). Figures in Sec. III cover this regime but the qualitative change in the eigenstate character has no visible effects on the relaxation rates (verified also for $2d/l_0 > 5$, not shown).

Next we considered direct transitions due to random nuclear fields without phonon assistance. Such transitions are possible if the eigenstates have unsharp energies (finite lifetimes). As the states we are interested in are low lying, even at finite temperature their energy broadening is so small that the resulting nuclear induced spin relaxation is negligible.

Finally, we considered the consequences of the random character of the nuclear field, which blurs the electron energies. This statistical, rather than quantum mechanical, uncertainty can be grasped roughly by convoluting the relaxation curves with a Gaussian with an appropriate width, depending on which parameter we change, defined ultimately by the energy $g\mu_B \mathbf{B}_{\text{nuc}}$. We find this width to be unnoticeable small—as an example, the extremely narrow peaks in Fig. 5 survive practically untouched by such smoothening. We conclude that unpolarized nuclear spins in natural or purified Si are not expected to be visible in any way in the electron relaxation.

The figures presented and results discussed in this article were for zero temperature. In our model, a finite temperature amounts solely to allowing for energy increasing transitions (phonon absorption), in addition to phonon emission processes only which are present at zero temperature. We analyzed this possibility, adopting a typical experimental value of 100 mK. We have not found any case where such additional transitions would change the relaxation rates in any significant way (figures not shown). Our conclusion from these investigations is that the relaxation character, most notably its anisotropies, will not be influenced by experimentally relevant sub-Kelvin temperatures.

ACKNOWLEDGMENTS

This work was supported by DFG under grant SPP 1285 and SFB 689. P.S. acknowledges support by metaQUTE ITMS NFP 26240120022, CE SAS QUTE, EU Project Q-essence, APVV-0646-10 and SCIEIX.

Appendix A: Analytical Calculation of Relaxation Rates

In this section we calculate the relaxation rate, Eq. (9), analytically adopting several approximations. The calculations prove useful to explain the physical mechanism and to verify our numerical results. The validity of the

approximations will be discussed afterwards. In the following, the hyperfine coupling is neglected.

Approximating the sum in Eq. (9) by an integral, and rewriting the δ -function with respect to the z component of \mathbf{Q} , we obtain ($i \neq j$)

$$\Gamma_{ij} = \frac{E_{ij}}{8\pi^2 \rho \hbar^2} \sum_{\lambda} \int d\mathbf{q} \int dQ_z \frac{Q}{c_{\lambda}^3 \bar{Q}_z^{\lambda}} |D_{\mathbf{Q}}^{\lambda}|^2 |M_{ij}|^2 \times [\delta(Q_z - \bar{Q}_z^{\lambda}) + \delta(Q_z + \bar{Q}_z^{\lambda})], \quad (\text{A1})$$

where $\bar{Q}_z^{\lambda} = \sqrt{E_{ij}^2/(\hbar^2 c_{\lambda}^2) - q^2}$. Assuming the validity of the dipole approximation, the matrix element reads

$$M_{ij} \approx i\langle i|\mathbf{q} \cdot (\mathbf{r}_1 + \mathbf{r}_2)|j\rangle, \quad (\text{A2})$$

where $|i\rangle$ and $|j\rangle$ are the spin-orbit coupled two electron eigenstates. Note that the contribution of the wave function overlap along the z direction in M_{ij} is about 1,⁹⁰ which is consistent with the two-dimensional approximation. We restrict ourselves to weakly coupled double dots, i.e. $d \gg l_0$, and incorporate the effect of spin-orbit coupling perturbatively via a Schrieffer-Wolff transformation.^{91–93} The eigenstates then read (l labels the electrons)

$$|i\rangle = e^{-iO} \left(|i\rangle_0 + \sum_k \sum_{l=1,2} \frac{0\langle k|\bar{H}_{\text{so},l}|i\rangle_0}{E_i^0 - E_k^0} |k\rangle_0 \right), \quad (\text{A3})$$

with the transformation operator $O = -\sum_l \mathbf{n}_{\text{so},l} \cdot \boldsymbol{\sigma}_l/2$, where

$$\mathbf{n}_{\text{so},l} = \left(\frac{x_l}{l_d} - \frac{y_l}{l_{\text{br}}}, \frac{x_l}{l_{\text{br}}} - \frac{y_l}{l_d}, 0 \right), \quad (\text{A4})$$

and the effective spin-orbit operator $\bar{H}_{\text{so},l} = \bar{H}_{\text{so},l}^Z + \bar{H}_{\text{so},l}^{(2)}$, where

$$\bar{H}_{\text{so},l}^Z = \frac{g}{2} \mu_B (\mathbf{n}_{\text{so},l} \times \mathbf{B}) \cdot \boldsymbol{\sigma}_l, \quad (\text{A5})$$

$$\bar{H}_{\text{so},l}^{(2)} = \frac{\hbar}{4m} \left(\frac{1}{l_d^2} - \frac{1}{l_{\text{br}}^2} \right) L_{z,l} \sigma_{z,l} + \text{const.} \quad (\text{A6})$$

Here, $L_z = l_z + (e/2)r^2 B_z$, where l_z is the operator of angular momentum. The states in Eq. (A3) labeled with subscript 0 are eigenstates of the Hamiltonian

$$H^0 = \sum_{i=1,2} (T_i + V_i + H_{Z,i}) + H_C, \quad (\text{A7})$$

their eigenenergies are denoted as E^0 . We use the Heitler-London ansatz⁴⁷ to approximate the eigenstates of Eq. (A7).

We use Eq. (A3) to evaluate the matrix element M_{ij} . It is straightforward to show that contributions from coupling within the lowest four-dimensional subspace, $\mathcal{M} = \{S, T_-, T_0, T_+\}$, are zero or exponentially suppressed in d/l_0 . As a result, the relaxation requires coupling via higher states. Neglecting the L_z contribution to the effective spin-orbit coupling, Eq. (A6), we obtain

$$\frac{M_{ij}}{ig\mu_B} = \sum_{k \notin \mathcal{M}} \sum_{l=1,2} \left[\frac{0\langle i | (\mathbf{n}_{\text{so},l} \times \mathbf{B}) \cdot \boldsymbol{\sigma}_l | k \rangle_0}{E_i^0 - E_k^0} 0\langle k | q_x x_1 + q_y y_1 | j \rangle_0 + \frac{0\langle k | (\mathbf{n}_{\text{so},l} \times \mathbf{B}) \cdot \boldsymbol{\sigma}_l | j \rangle_0}{E_j^0 - E_k^0} 0\langle i | q_x x_1 + q_y y_1 | k \rangle_0 \right]. \quad (\text{A8})$$

The singlet is symmetric with respect to the inversion operator I (point reflection in real space), the triplets are antisymmetric.⁸¹ Consequently, it follows from Eq. (A8) that, within the dipole approximation, the singlet-triplet transition is forbidden. We also find that Eq. (A8) forbids a $T_+ \leftrightarrow T_-$ transition because the effective spin-orbit operator, $\bar{H}_{\text{so},l}^Z$, acts on only one of the two electron spins. Let us now look at the transition between T_0 and T_{\pm} .

To evaluate Eq. (A8), we reduce the infinite sum over k to cover only states within the energy window of about the confinement energy, $\hbar^2/(ml_0^2)$. Additionally, we can exclude any singlet from the sum, because the electron-phonon operator does not act in spin space. What is left can be captured by the Heitler-London approach.

Let $|R0\rangle$ be the (orbital) ground state of a single dot shifted to the “right” by d , i.e. the Fock-Darwin state of the right dot with the principal quantum number $n = 0$ and the orbital quantum number $l = 0$. Analogously we define the ground state of the “left” dot. The properly symmetrized triplet lowest in energy is

$$|\Psi_T\rangle_0 = (|R0, L0\rangle - |L0, R0\rangle) \otimes |T\rangle / \sqrt{2}. \quad (\text{A9})$$

The orbitally excited triplets can be constructed analogously, using $|R1\rangle$, and $|L1\rangle$, the displaced Fock-Darwin states with $n = 0$ and $|l| = 1$:

$$|k_{\pm}\rangle_0 = (|R0, L1\rangle - |L1, R0\rangle \pm (|R1, L0\rangle - |L0, R1\rangle)) \otimes |T\rangle / 2. \quad (\text{A10})$$

Neglecting the wave function overlap of states localized in different quantum dots, we calculate the matrix elements $0\langle \Psi_T | x_1 | k_{\pm} \rangle_0$ and $0\langle \Psi_T | y_1 | k_{\pm} \rangle_0$ analytically, yielding

$$0\langle \Psi_T | x_1 | k_{+} \rangle_0 = l_0 / \sqrt{8}, \quad (\text{A11})$$

$$0\langle \Psi_T | y_1 | k_{+} \rangle_0 = \text{sgn}(l) i l_0 / \sqrt{8}, \quad (\text{A12})$$

and $0\langle \Psi_T | x_1 | k_{-} \rangle_0 = 0\langle \Psi_T | y_1 | k_{-} \rangle_0 = 0$. We use Eqs. (A11) and (A12) as an approximation for the matrix elements in Eq. (A8). We also require the matrix elements of Pauli matrices respecting the spin quantization axis along \mathbf{B} . They read

$$\begin{aligned} \langle T_{\pm} | \boldsymbol{\sigma}_1 | T_0 \rangle &= \\ &= \frac{e^{\mp i\gamma}}{2\sqrt{2}} \begin{pmatrix} \cos(\gamma - \theta) + \cos(\gamma + \theta) \pm 2i \sin(\gamma) \\ \sin(\gamma - \theta) + \sin(\gamma + \theta) \mp 2i \cos(\gamma) \\ 2 \sin(\theta) \end{pmatrix} \end{aligned} \quad (\text{A13})$$

where $\theta = \cos^{-1}(B_z/B_{\parallel})$. The energy differences in Eq. (A8) are approximated by the confinement energy, $\hbar^2/(ml_0^2)$.

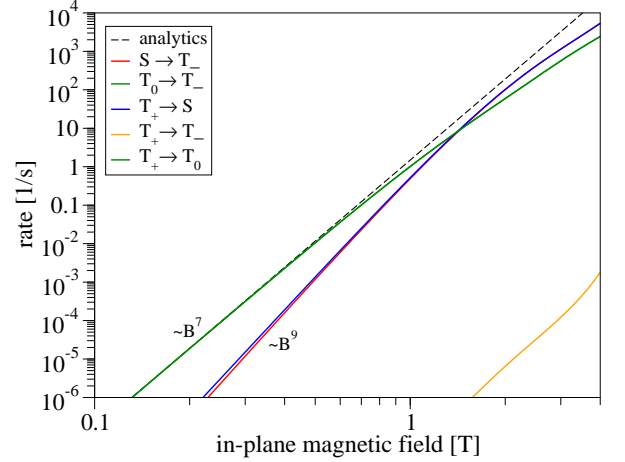


FIG. 10. (Color online) Calculated relaxation rates of individual transition channels as a function of in-plane magnetic field for a weakly coupled quantum dot. The magnetic field is orientated along $[\bar{1}10]$ ($\gamma = 3\pi/4$), and the dots along $[110]$ ($\delta = \pi/4$). The interdot distance is $2d/l_0 = 2.85$, yielding the tunneling energy $T = 0.1$ meV. The dashed, black line gives the analytical relaxation rate, evaluated with Eq. (A14).

With these ingredients, we can solve Eq. (A1), integrating over the phonon momentum, and obtain

$$\begin{aligned} \Gamma_{T_0 \rightarrow T_-} &= \Gamma_{T_+ \rightarrow T_0} = \frac{m^2 l_0^8 \mathcal{L}_{\text{so}}^{-2}}{12\pi \rho \hbar^{10}} (g\mu_B B)^7 \\ &\times [c_l^{-7} (\frac{3}{35} \Xi_u^2 + \frac{2}{5} \Xi_u \Xi_d + \Xi_d^2) + c_t^{-7} \frac{4}{35} \Xi_u^2], \end{aligned} \quad (\text{A14})$$

with the effective spin-orbit length \mathcal{L}_{so} , defined by

$$\mathcal{L}_{\text{so}}^{-2} = \begin{cases} 2(l_{\text{br}}^{-2} + l_d^{-2}) & \text{if } \theta = 0, \\ l_{\text{br}}^{-2} + l_d^{-2} - 2 \frac{\sin(2\gamma)}{l_{\text{br}} l_d} & \text{if } \theta = \pi/2. \end{cases} \quad (\text{A15})$$

Now we discuss the validity of the approximations used during the derivation of Eq. (A14). The matrix element M_{ij} is calculated using the dipole approximation, Eq. (A2). It requires that the energy difference between the transition states, here T_0 and T_{\pm} , fulfills $E_{ij} \ll \hbar c_{\lambda}/l_0$.⁹⁰ Using $E_{ij} = g\mu_B B$, and $c_{\lambda} = c_t$, we obtain the condition $B \ll 1.4$ T. We consider also a weakly coupled double dot, $d \gg l_0$, to comply with most experiments. This limit ensures negligible matrix elements among the states of \mathcal{M} , and justifies the Heitler-London approximation. Here, the spectrum also develops bundles of eigenenergies separated by the confinement energy $\hbar^2/(ml_0^2)$, a fact used to approximate the energy differences in Eq. (A8). Note that within the restriction of the dipole approximation ($B \ll 1.4$ T), the Zeeman energy ($E_Z \ll 0.16$ meV) is negligible compared to the confinement energy ($E_0 = 1$ meV). The Schrieffer-Wolff trans-

formation is the essential tool for a perturbative treatment of spin-orbit coupling in the double dot.⁸⁹ Perturbation theory with the unitarily transformed Hamiltonian yields results which are higher order in small quantities compared to the original Hamiltonian. Finally, we note that, since L_z is symmetric with respect to the inversion I , the perturbation $\bar{H}_{\text{so},l}^{(2)}$, Eq. (A6), vanishes for all transitions $T_0 \leftrightarrow T_{\pm}$.

We compare the analytical formula for the relaxation rate of the transition $T_0 \rightarrow T_-$, and $T_+ \rightarrow T_0$, given in Eq. (A14), with the numerical results in Fig. 10. We find

perfect agreement for low magnetic fields, in line with the condition $B \ll 1.4$ T. For larger magnetic fields, the results significantly deviate from the B^7 power law, due to the break down of the dipole approximation. We also find that the $S \leftrightarrow T_{\pm}$ relaxation channels, which we found to be zero in the lowest order dipole approximation due to their symmetry, show B^9 dependence, indicating that the relaxation is driven by the second order term of \mathbf{q} . Being of higher order, the relaxation rate, for small \mathbf{B} , is at least one order of magnitude lower than the $T_0 \leftrightarrow T_{\pm}$ transitions.

-
- ¹ D. Loss and D. P. DiVincenzo, Phys. Rev. A **57**, 120 (1998)
 - ² I. Žutić, J. Fabian, and S. Das Sarma, Rev. Mod. Phys. **76**, 323 (2004)
 - ³ J. Fabian, A. Matos-Abiague, C. Ertler, P. Stano, and I. Žutić, Acta Phys. Slov. **57**, 565 (2007), arXiv:0711.1461
 - ⁴ M. A. Nielsen and I. L. Chuang, *Quantum computation and quantum information* (Cambridge University, Cambridge, NY, 2000)
 - ⁵ R. Hanson and G. Burkard, Phys. Rev. Lett. **98**, 050502 (2007)
 - ⁶ G. Burkard, J. Phys.: Condens. Matter **19**, 233202 (2007)
 - ⁷ X. Hu and S. Das Sarma, Phys. Rev. A **61**, 062301 (2000)
 - ⁸ D. P. DiVincenzo, Fortschr. Phys. **48**, 771 (2000)
 - ⁹ T. D. Ladd, F. Jelezko, R. Laflamme, Y. Nakamura, C. Monroe, and J. L. O’Brien, Nature **464**, 45 (2010)
 - ¹⁰ R. Hanson, L. P. Kouwenhoven, J. R. Petta, S. Tarucha, and L. M. K. Vandersypen, Rev. Mod. Phys. **79**, 1217 (2007)
 - ¹¹ R. Brunner, Y.-S. Shin, T. Obata, M. Pioro-Ladrière, T. Kubo, K. Yoshida, T. Taniyama, Y. Tokura, and S. Tarucha, Phys. Rev. Lett. **107**, 146801 (2011)
 - ¹² J. M. Taylor, J. R. Petta, A. C. Johnson, A. Yacoby, C. M. Marcus, and M. D. Lukin, Phys. Rev. B **76**, 035315 (2007)
 - ¹³ M. Pioro-Ladrière, T. Obata, Y. Tokura, Y.-S. Shin, T. Kubo, K. Yoshida, T. Taniyama, and S. Tarucha, Nat. Phys. **4**, 776 (2008), ISSN 1745-2473
 - ¹⁴ T. Obata, M. Pioro-Ladrière, Y. Tokura, Y.-S. Shin, T. Kubo, K. Yoshida, T. Taniyama, and S. Tarucha, Phys. Rev. B **81**, 085317 (2010)
 - ¹⁵ A. V. Khaetskii and Y. V. Nazarov, Phys. Rev. B **64**, 125316 (2001)
 - ¹⁶ J. Schliemann, A. Khaetskii, and D. Loss, J. Phys: Condens. Matter **15**, R1809 (2003)
 - ¹⁷ J. R. Petta, A. C. Johnson, J. M. Taylor, E. A. Laird, A. Yacoby, M. D. Lukin, C. M. Marcus, M. P. Hanson, and A. C. Gossard, Science **309**, 2180 (2005)
 - ¹⁸ M. S. Rudner and L. S. Levitov, Phys. Rev. Lett. **99**, 036602 (2007)
 - ¹⁹ M. S. Rudner and L. S. Levitov, Phys. Rev. Lett. **99**, 246602 (2007)
 - ²⁰ H. Bluhm, S. Foletti, I. Neder, M. Rudner, D. Mahalu, V. Umansky, and A. Yacoby, Nat. Phys. **7**, 109 (2011), ISSN 1745-2473
 - ²¹ B. Braunecker, P. Simon, and D. Loss, Phys. Rev. B **80**, 165119 (2009)
 - ²² R. Hanson and D. D. Awschalom, Nature **453**, 1043 (2008), ISSN 0028-0836
 - ²³ G. Balasubramanian, P. Neumann, D. Twitchen, M. Markham, R. Kolesov, N. Mizuochi, J. Isoya, J. Achard, J. Beck, J. Tessler, V. Jacques, P. R. Hemmer, F. Jelezko, and J. Wrachtrup, Nature Mater. **8**, 383 (2009)
 - ²⁴ T. D. Ladd, D. Maryenko, Y. Yamamoto, E. Abe, and K. M. Itoh, Phys. Rev. B **71**, 014401 (2005)
 - ²⁵ J. J. L. Morton, D. R. McCamey, M. A. Eriksson, and S. A. Lyon, Nature **479**, 345 (2011), ISSN 0028-0836
 - ²⁶ J. W. Ager and E. E. Haller, physica status solidi (a) **203**, 3550 (2006)
 - ²⁷ J. Sailer, V. Lang, G. Abstreiter, G. Tsuchiya, K. M. Itoh, J. W. Ager, E. E. Haller, D. Kupidura, D. Harbusch, S. Ludwig, and D. Bougeard, Phys. Status Solidi RRL **3**, 61 (2009)
 - ²⁸ A. Wild, J. Kierig, J. Sailer, J. W. Ager, III, E. E. Haller, G. Abstreiter, S. Ludwig, and D. Bougeard, Appl. Phys. Lett. **100**, 143110 (2012)
 - ²⁹ M. G. Borselli, K. Eng, E. T. Croke, B. M. Maune, B. Huang, R. S. Ross, A. A. Kiselev, P. W. Deelman, I. Alvarado-Rodriguez, A. E. Schmitz, M. Sokolich, K. S. Holabird, T. M. Hazard, M. F. Gyure, and A. T. Hunter, Applied Physics Letters **99**, 063109 (2011)
 - ³⁰ B. M. Maune, M. G. Borselli, B. Huang, T. D. Ladd, P. W. Deelman, K. S. Holabird, A. A. Kiselev, I. Alvarado-Rodriguez, R. S. Ross, A. E. Schmitz, M. Sokolich, C. A. Watson, M. F. Gyure, and A. T. Hunter, Nature **481**, 344 (2012)
 - ³¹ J. R. Prance, Z. Shi, C. B. Simmons, D. E. Savage, M. G. Lagally, L. R. Schreiber, L. M. K. Vandersypen, M. Friesen, R. Joynt, S. N. Coppersmith, and M. A. Eriksson, Phys. Rev. Lett. **108**, 046808 (2012)
 - ³² E. P. Nordberg, G. A. T. Eyck, H. L. Stalford, R. P. Muller, R. W. Young, K. Eng, L. A. Tracy, K. D. Childs, J. R. Wendt, R. K. Grubbs, J. Stevens, M. P. Lilly, M. A. Eriksson, and M. S. Carroll, Phys. Rev. B **80**, 115331 (2009)
 - ³³ M. A. Eriksson, M. Friesen, S. N. Coppersmith, R. Joynt, L. J. Klein, K. Slinker, C. Tahan, P. M. Mooney, J. O. Chu, and S. J. Koester, Quantum Information Processing **3**, 133 (2004), ISSN 1570-0755
 - ³⁴ F. Schäffler, Semicond. Sci. Technol. **12**, 1515 (1997)
 - ³⁵ D. J. Paul, Semicond. Sci. Technol. **19**, R75 (2004)
 - ³⁶ M. S. Dresselhaus, G. Dresselhaus, and A. Jorio, *Group Theory: Application to the Physics of Condensed Matter*, 1st ed. (Springer, 2008)
 - ³⁷ T. Ando, A. B. Fowler, and F. Stern, Rev. Mod. Phys. **54**, 437 (1982)
 - ³⁸ T. Ando, Phys. Rev. B **19**, 3089 (1979)

- ³⁹ P. Weitz, R. Haug, K. von. Klitzing, and F. Schäffler, *Surf. Sci.* **361/362**, 542 (1996)
- ⁴⁰ S. Goswami, K. A. Slinker, M. Friesen, L. M. McGuire, J. L. Truitt, C. Tahan, L. J. Klein, J. O. Chu, P. M. Mooney, D. W. van der Weide, R. Joynt, S. N. Coppersmith, and M. A. Eriksson, *Nat. Phys.* **3**, 41 (2007)
- ⁴¹ A. L. Saraiva, M. J. Calderón, X. Hu, S. Das Sarma, and B. Koiller, *Phys. Rev. B* **80**, 081305 (2009)
- ⁴² D. Culcer, L. Cywiński, Q. Li, X. Hu, and S. Das Sarma, *Phys. Rev. B* **82**, 155312 (2010)
- ⁴³ M. Friesen, S. Chutia, C. Tahan, and S. N. Coppersmith, *Phys. Rev. B* **75**, 115318 (2007)
- ⁴⁴ M. Friesen and S. N. Coppersmith, *Phys. Rev. B* **81**, 115324 (2010)
- ⁴⁵ M. G. Borselli, R. S. Ross, A. A. Kiselev, E. T. Croke, K. S. Holabird, P. W. Deelman, L. D. Warren, I. Alvarado-Rodriguez, I. Milosavljevic, F. C. Ku, W. S. Wong, A. E. Schmitz, M. Sokolich, M. F. Gyure, and A. T. Hunter, *Applied Physics Letters* **98**, 123118 (2011)
- ⁴⁶ D. Culcer, L. Cywinski, Q. Li, X. Hu, and S. Das Sarma, *Phys. Rev. B* **80**, 205302 (2009)
- ⁴⁷ Q. Li, L. Cywinski, D. Culcer, X. Hu, and S. Das Sarma, *Phys. Rev. B* **81**, 085313 (2010)
- ⁴⁸ N. S. Lai, W. H. Lim, C. H. Yang, F. A. Zwanenburg, W. A. Coish, F. Qassemi, A. Morello, and A. S. Dzurak, *Sci. Rep.* **1** (2011)
- ⁴⁹ R. R. Hayes, A. A. Kiselev, M. G. Borselli, S. S. Bui, E. T. Croke, III, P. W. Deelman, B. M. Maune, I. Milosavljevic, J. Moon, R. S. Ross, A. E. Schmitz, M. F. Gyure, and A. T. Hunter, *arxiv:0908.0173*(unpublished)
- ⁵⁰ C. B. Simmons, J. R. Prance, B. J. Van Bael, T. S. Koh, Z. Shi, D. E. Savage, M. G. Lagally, R. Joynt, M. Friesen, S. N. Coppersmith, and M. A. Eriksson, *Phys. Rev. Lett.* **106**, 156804 (2011)
- ⁵¹ D. Culcer, A. L. Saraiva, B. Koiller, X. Hu, and S. Das Sarma, *Phys. Rev. Lett.* **108**, 126804 (2012)
- ⁵² M. Xiao, M. G. House, and H. W. Jiang, *Phys. Rev. Lett.* **104**, 096801 (2010)
- ⁵³ W. Pan, X. Z. Yu, and W. Z. Shen, *Appl. Phys. Lett.* **95**, 013103 (2009)
- ⁵⁴ A. Tyryshkin, S. Lyon, T. Schenkel, J. Bokor, J. Chu, W. Jantsch, F. Schäffler, J. Truitt, S. Coppersmith, and M. Eriksson, *Physica E* **35**, 257 (2006)
- ⁵⁵ C. Tahan, M. Friesen, and R. Joynt, *Phys. Rev. B* **66**, 035314 (2002)
- ⁵⁶ M. Prada, R. H. Blick, and R. Joynt, *Phys. Rev. B* **77**, 115438 (2008)
- ⁵⁷ B. A. Glavin and K. W. Kim, *Phys. Rev. B* **68**, 045308 (2003)
- ⁵⁸ M. Raith, P. Stano, and J. Fabian, *Phys. Rev. B* **83**, 195318 (2011)
- ⁵⁹ L. Wang and M. W. Wu, *J. Appl. Phys.* **110**, 043716 (2011)
- ⁶⁰ L. Wang, K. Shen, B. Y. Sun, and M. W. Wu, *Phys. Rev. B* **81**, 235326 (2010)
- ⁶¹ K. Shen and M. W. Wu, *Phys. Rev. B* **76**, 235313 (2007)
- ⁶² E. Y. Sherman and D. J. Lockwood, *Phys. Rev. B* **72**, 125340 (2005)
- ⁶³ F. A. Zwanenburg, A. S. Dzurak, A. Morello, M. Y. Simmons, L. C. L. Hollenberg, G. Klimeck, S. Rogge, S. N. Coppersmith, and M. A. Eriksson, *arxiv:1206.5202*(unpublished)
- ⁶⁴ J. Fabian and S. Das Sarma, *Phys. Rev. Lett.* **81**, 5624 (1998)
- ⁶⁵ M. Raith, P. Stano, F. Baruffa, and J. Fabian, *Phys. Rev. Lett.* **108**, 246602 (2012)
- ⁶⁶ P. Stano and J. Fabian, *Phys. Rev. Lett.* **96**, 186602 (2006)
- ⁶⁷ M. Raith, Diploma Thesis, University of Regensburg, Germany, 2009
- ⁶⁸ J. Pedersen, C. Flindt, N. A. Mortensen, and A.-P. Jauho, *Phys. Rev. B* **76**, 125323 (2007)
- ⁶⁹ P. Stano and J. Fabian, *Phys. Rev. B* **77**, 045310 (2008)
- ⁷⁰ Y. A. Bychkov and E. I. Rashba, *J. Phys. C* **17**, 6039 (1984)
- ⁷¹ G. Dresselhaus, *Phys. Rev.* **100**, 580 (1955)
- ⁷² L. E. Golub and E. L. Ivchenko, *Phys. Rev. B* **69**, 115333 (2004)
- ⁷³ M. O. Nestoklon, E. L. Ivchenko, J.-M. Jancu, and P. Voisin, *Phys. Rev. B* **77**, 155328 (2008)
- ⁷⁴ L. V. C. Assali, H. M. Petrilli, R. B. Capaz, B. Koiller, X. Hu, and S. Das Sarma, *Phys. Rev. B* **83**, 165301 (2011)
- ⁷⁵ A. Khaetskii, D. Loss, and L. Glazman, *Phys. Rev. B* **67**, 195329 (2003)
- ⁷⁶ C. Herring and E. Vogt, *Phys. Rev.* **101**, 944 (1956)
- ⁷⁷ H. Hasegawa, *Phys. Rev.* **118**, 1523 (1960)
- ⁷⁸ E. Pop, R. W. Dutton, and K. E. Goodson, *J. Appl. Phys.* **96**, 4998 (2004)
- ⁷⁹ M. Dür, A. D. Gunther, D. Vasileska, and S. M. Goodnick, *Nanotechnology* **10**, 142 (1999)
- ⁸⁰ A. Grodecka, L. Jacak, P. Machnikowski, and K. Roszak, *Quantum Dots: Research Developments* (Nova Science, NY, 2005) *arXiv:cond-mat/0404364*
- ⁸¹ F. Baruffa, P. Stano, and J. Fabian, *Phys. Rev. Lett.* **104**, 126401 (2010)
- ⁸² F. Baruffa, P. Stano, and J. Fabian, *Phys. Rev. B* **82**, 045311 (2010)
- ⁸³ L. Yang, J. R. Watling, R. C. W. Wilkins, M. Borii, J. R. Barker, A. Asenov, and S. Roy, *Semiconductor Science and Technology* **19**, 1174 (2004)
- ⁸⁴ M. M. Rieger and P. Vogl, *Phys. Rev. B* **48**, 14276 (1993)
- ⁸⁵ H. Malissa, W. Jantsch, M. Muhlberger, F. Schaffler, Z. Wilamowski, M. Draxler, and P. Bauer, *Applied Physics Letters* **85**, 1739 (2004)
- ⁸⁶ O. Madelung, U. Rössler, and M. Schulz, *Landolt-Börnstein - Group III Condensed Matter*, Vol. 41A1b (Springer, Berlin, 2002)
- ⁸⁷ M. V. Fischetti and S. E. Laux, *J. Appl. Phys.* **80**, 2234 (1996)
- ⁸⁸ D. S. Gandolfo, D. A. Williams, and H. Qin, *J. Appl. Phys.* **97**, 063710 (2005)
- ⁸⁹ P. Stano and J. Fabian, *Phys. Rev. B* **72**, 155410 (2005)
- ⁹⁰ P. Stano and J. Fabian, *Phys. Rev. B* **74**, 045320 (2006)
- ⁹¹ P. Löwdin, *J. Chem. Phys.* **19**, 1396 (1951)
- ⁹² J. R. Schrieffer and P. A. Wolff, *Phys. Rev.* **149**, 491 (1966)
- ⁹³ R. Winkler, *Spin-Orbit Coupling Effects in Two-Dimensional Electron and Hole Systems*, 1st ed. (Springer, 2003)